JOURNAL OF AIRCRAFT
Vol. 31, No. 2, March–April 1994

Prediction of Ice Shapes and Their Effect on Airfoil Drag

Jaiwon Shin*
National Aeronautics and Space Administration, Cleveland, Ohio 44135
Brian Berkowitz†
Sverdrup Technology, Inc., Brook Park, Ohio 44142
and
Hsun H. Chen‡ and Tuncer Cebeci§
California State University, Long Beach, California 90840

Calculation of ice shapes and the resulting drag increases are presented for a NACA 0012 airfoil. The calculations were made using a combination of modified LEWICE and interactive boundary-layer codes for a wide range of values of parameters such as airspeed and temperature, the droplet size and liquid water content of the cloud, and the angle of attack of the airfoil. Based on experimental data, an improved correlation of equivalent sand-grain roughness was developed. Calculated ice shapes are in good agreement with experimental data for rime ice, but some differences are shown between predictions and experimental data for glaze ice. Calculated drag coefficients generally follow trends shown by the experimental data.

Nomenclature

A = damping-length constant
C_D = drag coefficient
c = airfoil chord length, m
c_{ij} = interaction-coefficient matrix
k_s = equivalent sand-grain roughness
k_s^+ = dimensionless sand-grain roughness
L = mixing length
T_s = static air temperature, °C
u = streamwise velocity component, m/s
u_e = boundary-layer edge velocity, m/s
u_e^0 = inviscid velocity
u_e^κ = inviscid velocity which contains the displacement effect from a previous sweep
u_τ = friction velocity
V_n = blowing velocity
V_∞ = airspeed, m/s
x = distance along the surface, m
x_a, x_b = range of the viscous/inviscid interaction region, m
y = distance normal to the surface, m
y^+ = Reynolds number, yu_τ/ν
α = angle of attack, deg
δ^* = displacement thickness
δu_e = perturbation velocity due to viscous effects
κ = universal constant, also used as a sweep parameter
ν = kinematic viscosity, m²/s
σ = source strength

Presented as Paper 91-0264 at the AIAA 29th Aerospace Sciences Meeting, Reno, NV, Jan. 7–10, 1991; received Oct. 7, 1991; revision received Dec. 18, 1992; accepted for publication Dec. 20, 1992.

*Aerospace Engineer, Icing and Cryogenic Technology Branch, Propulsion Systems Division. Member AIAA.
†Aircraft Icing Engineer, Lewis Research Center Group.
‡Associate Professor, Aerospace Engineering Department. Member AIAA.
§Professor and Chairman, Aerospace Engineering Department. Fellow AIAA.

Introduction

THE prediction of ice shapes and their effect on lifting surfaces is a problem of central importance in aircraft design since ice accretion can adversely affect aerodynamic performance of aircraft components. In recent years, research has been undertaken to improve understanding of the formation of the ice, its accretion, and the consequences for aerodynamic performance. Reference 1 provides an overview of the analytical and experimental icing activities in progress, and Ref. 2 provides a review of the progress on one element of the overall activity, namely the unprotected airfoil icing problem. The latter discusses the development and validation of computer codes which predict the buildup of ice on unprotected airfoils and the resulting degradation of aerodynamic performance due to ice accretion.

These state-of-the-art reviews show that a two-dimensional ice accretion code, LEWICE, developed in 1983 at the University of Dayton Research Institute,[3] and later modified by Ruff,[4] provides a basis for the determination of the ice buildup on the leading edge of airfoils for both the glaze ice formed at temperatures slightly below freezing and at relatively high liquid water contents and high flight speeds and for the rime ice which occurs at low temperatures, low liquid water contents, and low flight speeds. The three major elements of this code are 1) an inviscid panel code, 2) a water droplet trajectory model, and 3) an energy balance equation proposed by Messinger.[5] The ice accretion is computed on the airfoil leading edge as a function of time with user specified time intervals. At each given time, the inviscid flowfield is determined from the panel code so that trajectory and heat transfer calculations can be performed. As the ice accretion builds up, its shape may become rugged, especially in the case of glaze ice which is characterized by horns, and a rough, irregular surface, and leads to higher aerodynamic losses unlike the rime ice. Surface irregularities of the ice shape can lead to multiple stagnation points with subsequent numerical difficulties, including a breakdown of the trajectory calculations which are necessary to determine the spatial distribution of water droplets. The automated smoothing procedure[6] overcomes this difficulty by reducing the amplitude of the surface irregularities without loss of important flow characteristics, and usually allows the calculations to be performed for greater times than before, without the problems caused by multiple stagnation points.

In addition to the need to predict ice shapes accurately, it is important to determine the performance degradation of the airfoil due to icing. This can be achieved by two codes based on solutions of the Reynolds-averaged Navier-Stokes equations and their reduced forms. The Navier-Stokes method employs the ARC-2D code and has been developed for iced airfoils by Potapczuk.[7] The interactive boundary-layer (IBL) method of Cebeci[8] combines the solutions of the inviscid and viscous flow equations with an interaction law based on the Hilbert integral. The latter method has been incorporated into the LEWICE code so that ice shapes and performance degradation of the airfoil can be predicted.

This article applies the combination of the modified LEWICE code (one with the smoothing procedure) and the IBL method to predict ice shapes and their effect on airfoil drag. The following section presents a brief description of the interactive boundary-layer procedure. The calculated and measured ice shapes and the resulting drag increase are compared for an NACA 0012 airfoil. The experimental data is due to Olsen et al.[9] and was obtained in the NASA Icing Research Tunnel (IRT). The measurements were made over a large range of airspeed and temperature, the droplet size and liquid water content of the cloud, and the angle of attack of the airfoil. This article ends with a brief discussion of the implications of the results and a summary of the more important conclusions.

Description of the Interactive Boundary-Layer Method

The original LEWICE code is described in detail in Ref. 4, and an operator-free procedure incorporated into this code in order to avoid the occurrence of the multiple stagnation points caused by the formation of irregular surfaces on the ice shape is discussed in Ref. 6. For this reason, the following description of the interactive boundary-layer procedure is brief. The IBL method couples the solutions of inviscid and viscous flow equations so as to ensure that each influences the other. The inviscid flow equations are solved by a panel method in which the airfoil and ice shapes are defined by a set of points where neighboring points are connected by straight-line panels which each have source density and vorticity. The vorticity strength of each panel is the same so that vorticity is defined by a total strength, adjusted to satisfy the Kutta condition. The source strengths have independent values on each panel, and these are adjusted by solving a set of simultaneous linear equations to satisfy the normal-velocity boundary condition at the midpoints of the panels. In the strictly inviscid case, this condition requires that the total normal velocity, freestream plus body sources and vortices, should vanish. When the boundary layer is simulated, the desired normal velocity, V_n, is finite and equals the derivative along the surface of the product of tangential velocity and displacement thickness, $d(u_e\delta^*)/dx$. It is known that this surface blowing distribution displaces the dividing streamline outward from the surface of the airfoil to the location of the displacement thickness. Experience has shown that best results are obtained when surface pressures are calculated and the Kutta condition is applied on the displacement surface rather than on the surface panels.

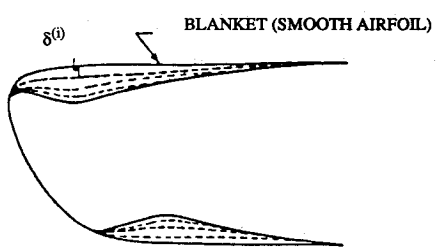

Fig. 1 Boundary-layer model used in the viscous-flow calculations.

The boundary-layer equations for two-dimensional external steady incompressible flows are well known and are solved with the Reynolds shear stress term modeled with the Cebeci-Smith eddy-viscosity formulation.[10] For the external velocity distribution specified by the panel method, $u_e^0(x)$, and with $\delta u_e(x)$ representing the perturbation velocity due to viscous effects, the edge boundary condition is written as

$$u_e(x) = u_e^0(x) + \delta u_e(x) \tag{1}$$

where, for the interaction region confined to the range $x_a \leq x \leq x_b$, which is often taken to include the airfoil chord length plus two chord lengths from the trailing edge

$$\delta u_e(x) = \frac{1}{\pi}\int_{x_a}^{x_b} \frac{d}{d\sigma}(u_e\delta^*)\frac{d\sigma}{x-\sigma} \tag{2}$$

with $d(u_e\delta^*)/d\sigma$ corresponding to the blowing velocity.

In this form, Eq. (1) provides an outer boundary condition for the viscous-flow calculations which represents the viscous/inviscid interaction and can be generalized to the form

$$u_e(x) = u_e^\kappa(x) + \sum_{j=1}^{n} c_{ij}[(u_e\delta^*)_j - (u_e\delta^*)_j^\kappa] \tag{3}$$

where $u_e^\kappa(x)$ corresponds to the inviscid velocity distribution which contains the displacement thickness effect $(\delta^*)^\kappa$ computed from a previous sweep. Here, c_{ij} is obtained from a discrete approximation to the Hilbert integral.

Ice on airfoils can introduce substantial geometric changes to their leading edges in a short period and cause rapid variations in the flow properties. As a result, the inviscid and viscous flow calculations may have difficulty in producing satisfactory solutions. For the boundary-layer calculations, the iced airfoil is regarded as a smooth or a rough surface obtained by covering the leading-edge region with a "blanket" as shown in Fig. 1. It also makes use of a continuation method in which the initial calculations are performed for the smooth airfoil, and subsequent ones for a series of shapes that fall between the "smooth" and iced airfoils. For each shape, the blowing velocity is computed from

$$V_n = \frac{d}{dx}[u_e(\delta^* - \delta)] \tag{4}$$

where δ^* corresponds to the displacement thickness obtained from the boundary-layer solutions for the shape whose geometrical difference from the smooth airfoil is $\delta^{(i)}(x)$, and where the δ^* surface is outside the singularity surface. This allows the viscous effects to be incorporated into the inviscid flow solutions gradually, at each time step, thus reducing the sensitivity of the viscous flow solutions to the rapid changes in the pressure distribution near the leading edge. For further details, see Ref. 6.

The numerical solutions of the boundary-layer equations, written in transformed variables, are obtained with the box method for both standard (prescribed pressure distribution) and interactive methods. This second-order finite-difference method has been used extensively by Cebeci and his associates for a wide range of flows.[10] An inverse form of the equations is used to obtain the solutions with separation and the FLARE approximation, in which the convective term $u(\partial u/\partial x)$ is set equal to zero in the recirculating region, is employed. The nonlinear system of algebraic equations which results from the finite-difference approximation is linearized by Newton's method and solved by a block elimination procedure. It should be noted that the mixing length expression of the Cebeci-Smith model[8] has been modified to deal with surface rough-

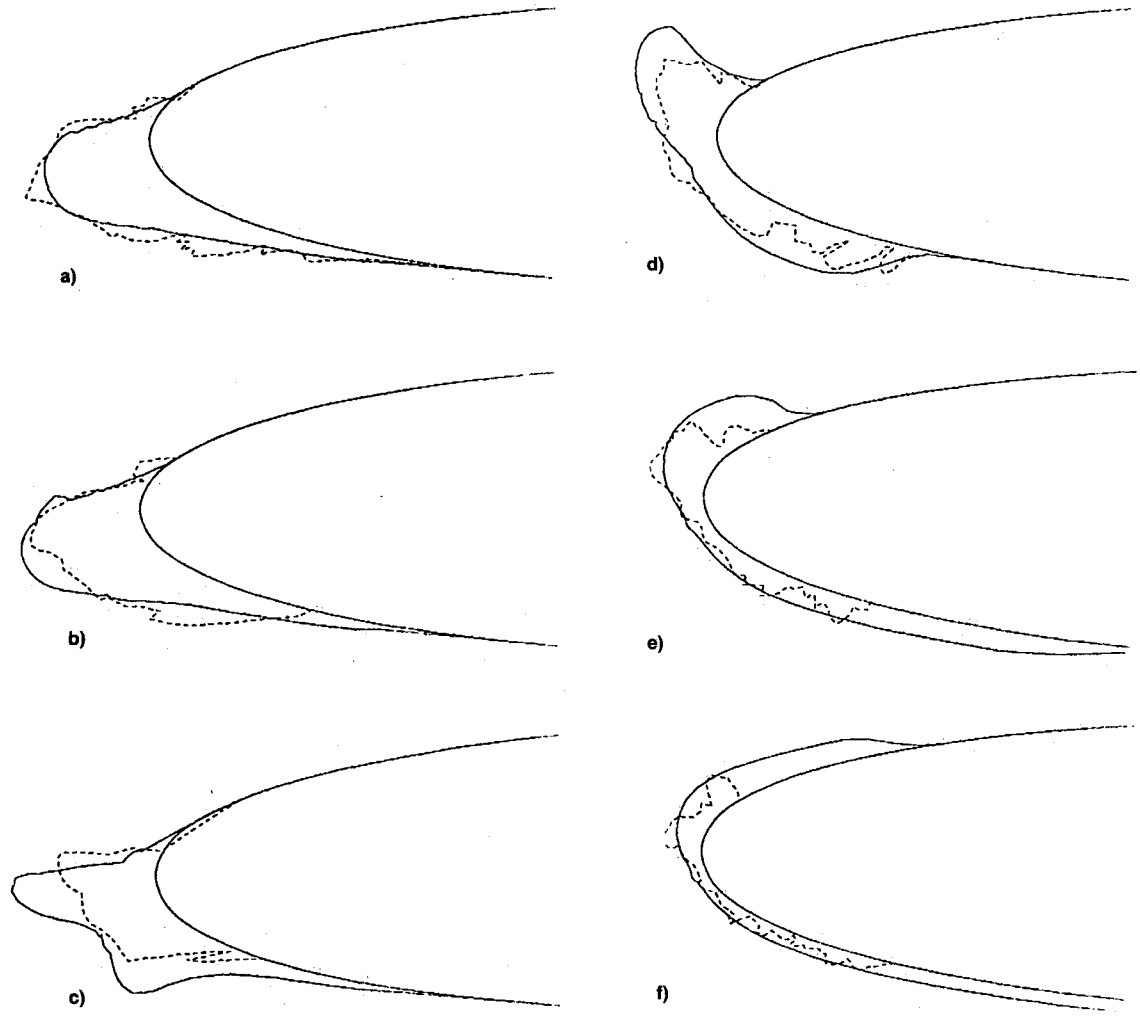

Fig. 2 Effect of T_s on ice shapes for fixed droplet size (MVD = 20 μm), air velocity (V_∞ = 58 m/s), liquid water content (LWC = 1.3 g/m^3): a) −27.8°C, b) −19.8°C, c) −13.9°C, d) −6.7°C, e) −3.9°C, and f) −2.8°C. All calculations are for 8 min, except for that of a) which is for 7 min. —— Predicted; --- measured (Ref. 9).

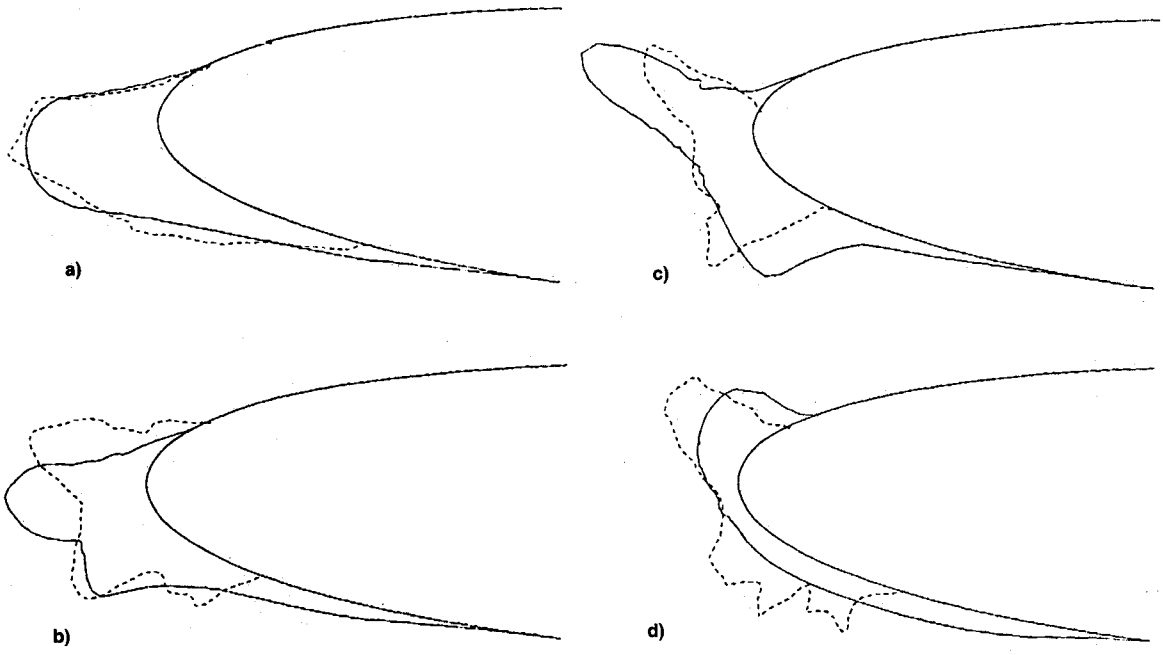

Fig. 3 Effect of T_s on ice shapes for fixed droplet size (MVD = 20 μm), air velocity (V_∞ = 94 m/s), liquid water content (LWC = 1.05 g/m^3): a) −30.5°C, b) −16.6°C, c) −12.2°C, and d) −6.6°C. All calculations are for 6.2 min, except for that of and d) which is for 4.13 min. —— Predicted; --- measured (Ref. 9).

ness, such as that associated with ice. This was done by modifying the mixing length and wall-damping expression, i.e.

$$L = 0.4(y + \Delta y)\{1 - \exp[-(y + \Delta y)/A]\} \qquad (5)$$

where Δy is a function of k_s. In terms of dimensionless quantities, with $k_s^+ (\equiv k_s u_\tau/\nu)$ and $\Delta y^+ (\equiv \Delta y u_\tau/\nu)$

$$\Delta y^+ = \begin{bmatrix} 0.9[\sqrt{k_s^+} - k_s^+ \exp(-k_s^+/6)], & 5 \le k_s^+ \le 70 \\ 0.7(k_s^+)^{0.58} & , \quad 70 \le k_s^+ \le 2000 \end{bmatrix} \qquad (6)$$

The equivalent sand-grain roughness for ice is determined from the expressions used in the LEWICE code, as discussed in the following section.

Results and Discussion

The computer program described in Ref. 6 has the option of computing the flowfield without and with viscous effects. Studies conducted with this code show that viscosity does not have a pronounced effect on the prediction of ice shapes. Even though the viscous flowfield differs significantly from that computed with a panel method, especially near the leading edge, the computed shapes remain relatively unchanged because of the insensitivity of the current heat transfer model to viscous corrections. As a result, all ice shape calculations, presented herein, are performed with the inviscid panel method.

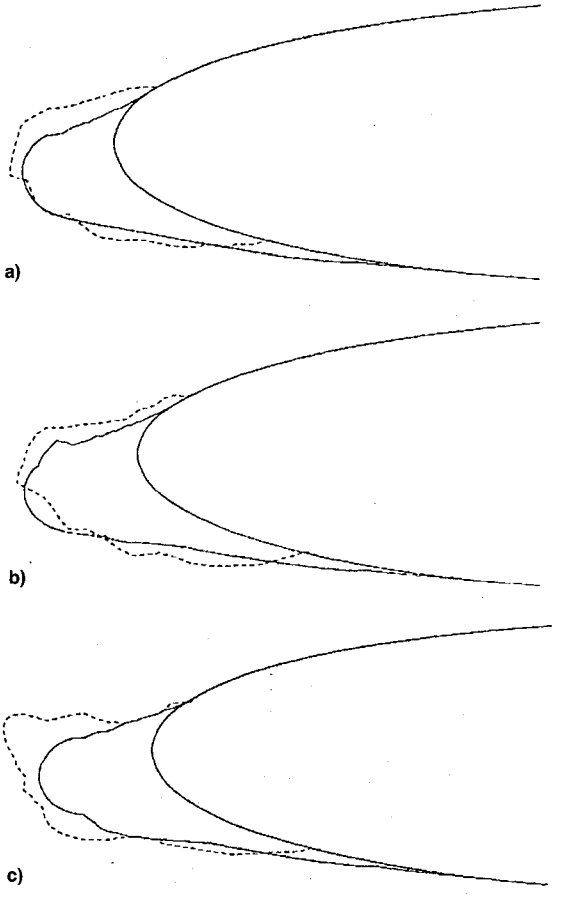

Fig. 4 Effect of LWC (g/m³), on ice shapes for fixed droplet size (MVD = 20 μm), air velocity (V_∞ = 58 m/s), air temperature (T_s = −19.8°C): a) 1.0, b) 1.3, and c) 2.0. All calculations are for 8 min, except for that of c) which is for 6 min. —— Predicted; --- measured (Ref. 9).

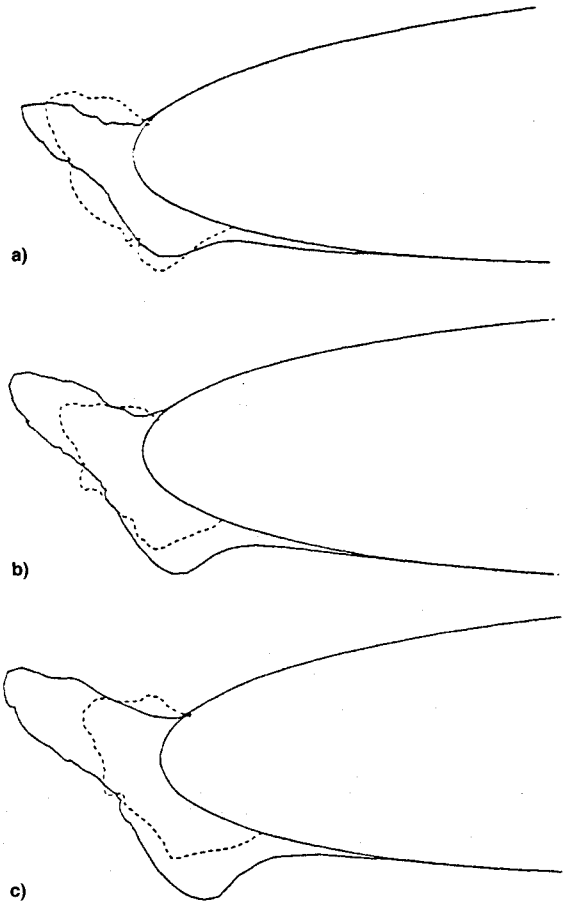

Fig. 5 Effect of LWC (g/m³), on ice shapes for fixed droplet size (MVD = 20 μm), air velocity (V_∞ = 58 m/s), air temperature (T_s = −9.67°C): a) 1.0, b) 1.3, and c) 1.6. All calculations are for 8 min. —— Predicted; --- measured (Ref. 9).

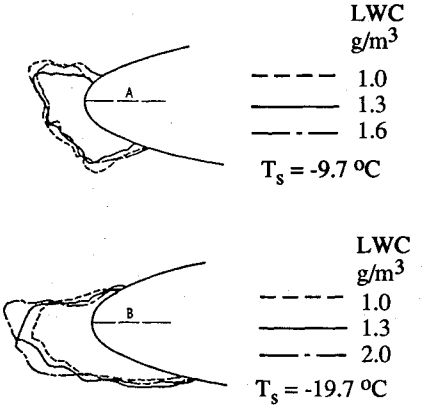

Fig. 6 Effect of LWC on the ice shape and section drag. V_∞ = 58 m/s, MVD = 20 μm, t = 8 min at 4-deg angle of attack (Ref. 9).

Before we compare the calculated and measured results, it is useful to review the extensive data of Olsen et al.[9] for a 0.53-m chord NACA 0012 airfoil. The experimental data includes ice shapes and the resulting drag coefficients, and were obtained over a range of air temperature, airspeed, airfoil angle of attack, spray time, liquid water content (LWC), and droplet size. The data are very informative and helpful, not only in understanding the ice structure and the way it forms, but it is also very useful in the development of computer codes such as the LEWICE and IBL codes to predict the ice accretion and resulting drag.

The heat transfer model used in the LEWICE code makes use of k_s, expressed as a function of LWC, T_s, and V_∞ in order

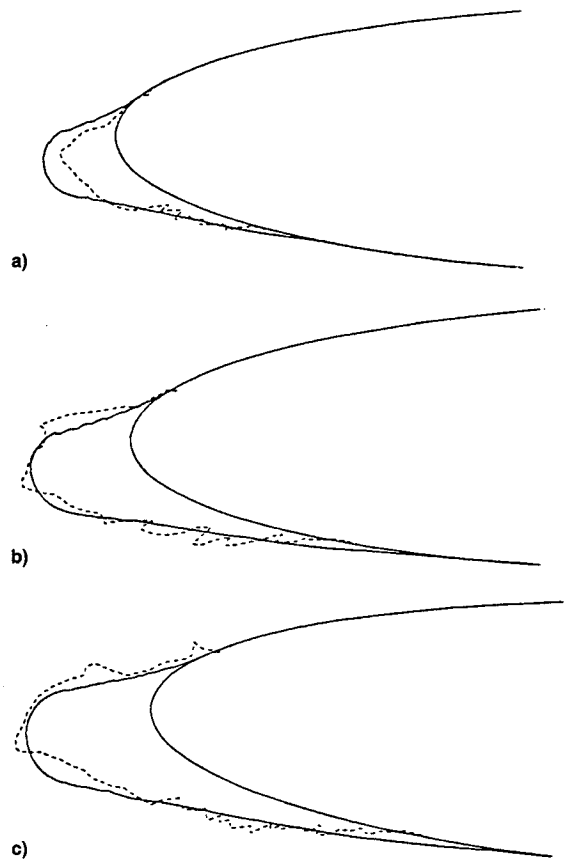

Fig. 7 Effect of droplet size MVD (μm), on ice shapes for fixed air velocity (V_∞ = 58 m/s), air temperature (T_s = −27.8°C), liquid water content (LWC = 1.30 g/m³): a) 14, b) 20, and c) 26. All calculations are for 7 min, except for that of c) which is for 8 min. —— Predicted; --- measured (Ref. 9).

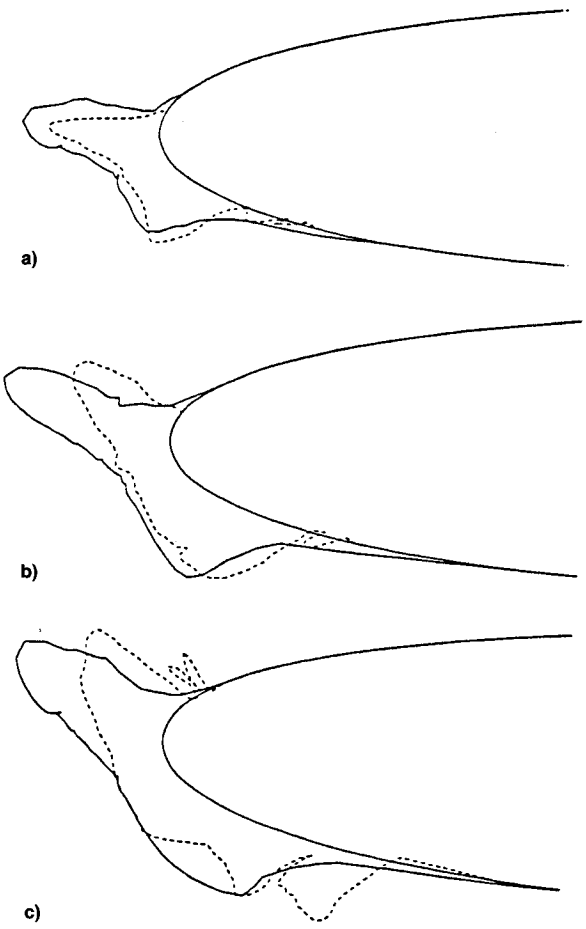

Fig. 8 Effect of droplet size MVD (μm), on ice shapes for fixed air velocity (V_∞ = 94 m/s), air temperature (T_s = −12.2°C), liquid water content (LWC = 1.05 g/m³): a) 14, b) 20, and c) 26. All calculations are for 6.2 min. —— Predicted; --- measured (Ref. 9).

to determine the ice shapes. With c denoting the airfoil chord and $(k_s/c)_{\text{base}} = 0.001177$, it is expressed in the following form:

$$k_s = \left[\frac{k_s/c}{(k_s/c)_{\text{base}}}\right]_{\text{LWC}} \cdot \left[\frac{k_s/c}{(k_s/c)_{\text{base}}}\right]_{T_s} \cdot \left[\frac{k_s/c}{(k_s/c)_{\text{base}}}\right]_{V_\infty} \cdot \left(\frac{k_s}{c}\right)_{\text{base}} \cdot c \tag{7}$$

where each sand-grain roughness parameter is given by

$$\left[\frac{k_s/c}{(k_s/c)_{\text{base}}}\right]_{\text{LWC}} = 0.5714 + 0.2457\ (\text{LWC}) + 1.2571\ (\text{LWC})^2 \tag{8a}$$

$$\left[\frac{k_s/c}{(k_s/c)_{\text{base}}}\right]_{T_s} = 0.047T_s - 11.27 \tag{8b}$$

$$\left[\frac{k_s/c}{(k_s/c)_{\text{base}}}\right]_{V_\infty} = 0.4286 + 0.0044139V_\infty \tag{8c}$$

These expressions are empirical, are based on experimental data reported in Ref. 4, and do not account for the effect of time on the ice roughness. The experimental data of Olsen et al.[9] shows that for the glaze ice condition, the roughness increases with time—rapidly at first—then more slowly. Their data also shows that rime ice is never as rough as glaze ice.

This experimental data was obtained at two airspeeds V_∞ corresponding to 58 and 94 m/s. The data shows that the roughness is nearly independent of V_∞ of 58 and 94 m/s, and that k_s is also a function of the median volume droplet (MVD) size, as well as a function of the parameters in Eq. (7). Based on these experimental observations, it is plausible to write Eq. (7) as

$$k_s = \left[\frac{k_s/c}{(k_s/c)_{\text{base}}}\right]_{\text{LWC}} \cdot \left[\frac{k_s/c}{(k_s/c)_{\text{base}}}\right]_{T_s} \cdot \left[\frac{k_s/c}{(k_s/c)_{\text{base}}}\right]_{V_\infty} \cdot \left[\frac{k_s/c}{(k_s/c)_{\text{base}}}\right]_{\text{MVD}} \cdot \left(\frac{k_s}{c}\right)_{\text{base}} \cdot c \tag{9}$$

with

$$\left[\frac{k_s/c}{(k_s/c)_{\text{base}}}\right]_{\text{MVD}} = \begin{cases} 1 & , \ \text{MVD} \le 20 \\ 1.667 - 0.0333\ \text{MVD}, & \text{MVD} > 20 \end{cases} \tag{10}$$

Some numerical studies conducted with the LEWICE code showed that the calculated results agreed better with experiment if the roughness parameter for V_∞ was taken as a constant 0.6839 corresponding to V_∞ of 58 m/s. Therefore, all subsequent calculations were performed with this assumption.

An appropriate k_s is also required in the turbulence model in the IBL code in order to compute the boundary-layer development on the airfoil and in the wake. It is plausible to conjecture that this parameter, as in the heat transfer model, is a function of LWC, V_∞, T_s, and MVD. For this reason, calculations with k_s corresponding to that used for the heat transfer model, Eq. (9) were performed with the IBL code for an ice shape determined with the LEWICE code. As

expected, the drag coefficients calculated from the wake velocity profiles indicated that the results were sensitive to the magnitude of the roughness parameter. Several calculations with the value of k_s of Eq. (9), multiplied by a constant equal to 2, yielded the best agreement with experiment. As a result, all boundary-layer calculations in the IBL code used a roughness parameter, $(k_s)_{IBL}$, given by

$$(k_s)_{IBL} = 2(k_s)_{Eq.(9)} \tag{11}$$

The following subsection presents the results for the ice shapes determined with the LEWICE code and obtained for a range of conditions which include V_∞, T_s, MVD, and LWC, all for a given angle of attack of 4 deg, and compares them with the measured shapes. As stated earlier, these calculations were performed with the flowfield computed with the inviscid panel code. Comparisons between the calculated and measured drag coefficients, again for a range of conditions as above plus the angle-of-attack effect, are presented in the following. In this case, the flowfield calculations on the airfoil and in the wake were performed in an interactive manner for the given calculated ice shapes, as discussed in the previous section.

Comparison Between Calculated and Measured Ice Shapes

Calculations were performed with the LEWICE code in order to determine the effects of T_s, LWC, and droplet size on ice shapes for the experimental data of Olsen et al.[9] The calculated and experimental results are shown by solid and dotted lines, respectively, in Figs. 2–8. Those shown in Figs. 2 and 3 indicate the effect of air temperature on the ice accretion and, in general, show promising agreement with data for two airspeeds. At low temperatures, when ice shapes correspond to rime ice, the comparisons between calculated and measured ice shapes are good. The comparison between calculated and measured ice shapes starts to show some differences as ice shapes change from rime to glaze for both airspeeds. Except for one case in each figure, the calculations were performed without numerical difficulties for the stated times of ice accretion in the experiments, which were 8 min for those in Fig. 2 and 6.2 min for those in Fig. 3.

The results in Figs. 4 and 5 show the effect of LWC on ice shapes. Those in a and b of each figure are for values of LWC of 1.0 and 1.3, respectively, and are in good agreement with experiment, although the ice shapes of b are not as good as those of a. For higher values of LWC, Figs. 4c and 5c, the agreement between measured and computed ice shapes worsens. The results are not unexpected because the correlations for the roughness parameter for LWC used in Ref. 4 are for a range of LWC up to 1.0 g/m^3. Furthermore, the experimental data (see also Fig. 6, taken from Ref. 9) indicate that, for values of LWC ranging from 1.0 to 2, the effect of LWC on the ice shape is negligible, and this suggests that the roughness parameter for LWC should be nearly constant. Ice shapes in Fig. 5 show those of typical glaze ice, and the agreement between predicted and measured shapes is not as good as that shown in Fig. 4 for rime ice. The calculations for the highest value of LWC also indicate some numerical difficulties with solutions breaking down after ice accretion time of 6 min, rather than the specified time of 8 min. A better correlation may improve the predicted ice shapes and avoid numerical difficulties.

Figs. 7 and 8 show the effect of droplet size on the ice shapes, again for two airspeeds and different temperatures. These results are generally in good agreement with data and are much better than those which did not include Eq. (10) in the calculations.

Table 1 Effect of air temperature on drag coefficient

Static air temperature, °C	Calculated drag coefficient	Experimental drag coefficient	Equivalent sand-grain roughness, mm
	(A)		
−27.8	0.01279	0.01941	0.334
−19.8	0.01346	0.02161	0.815
−13.9	0.01431	0.02072	1.170
−6.7	0.05075	0.06036	1.602
−3.9	0.02873	0.02807	1.770
−2.8	0.02105	0.02647	1.837
	(B)		
−30.5	0.01143	0.02380	0.126
−16.6	0.01300	0.03700	0.740
−12.2	0.04549	0.06060	0.934
−6.6	Breakdown	0.07560	1.182

(A) Airspeed = 58 m/s, LWC = 1.3 g/m^3, MVD = 20 μm, accretion time = 8 min.
(B) Airspeed = 94 m/s, LWC = 1.05 g/m^3, MVD = 20 μm, accretion time = 6.2 min.

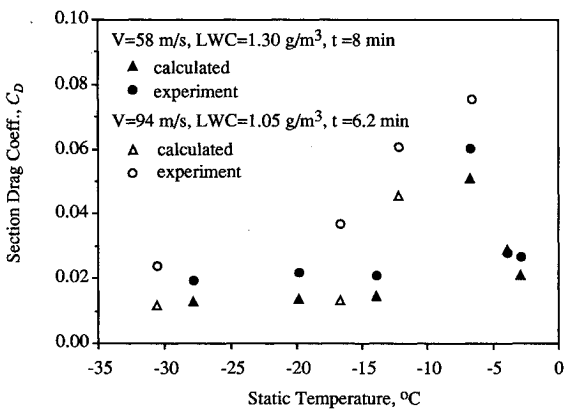

Fig. 9 Variation of the drag coefficient with static temperature at two airspeeds.

Drag Coefficients

At first the calculations were performed to investigate the effects of droplet size, LWC, and air temperature on the total drag coefficients of the airfoil. The ice shape determined at an angle of attack of 4 deg with the procedure described above was fixed in the calculations. Tables 1–3 show the results obtained in this manner.

Tables 1(A) and 1(B) show the effect of air temperature on drag coefficient for ice accretion times of 8 and 6.2 min for two airspeeds, respectively, together with the variation of k_s with temperature. Figure 9 shows the variation of the drag coefficient as a function of static air temperature and corresponds to the results of Table 1. As can be seen, at lower temperatures where the ice accretion leads to the formation

Table 2 Effect of liquid water content on drag coefficient

Liquid water content, g/m^3	Calculated drag coefficient	Experimental drag coefficient	Equivalent sand-grain roughness, mm
	(A)		
1.0	0.01398	0.02120	0.561
1.3	0.01346	0.02460	0.815
2.0	Breakdown	0.03120	1.647
	(B)		
1.0	0.02976	0.02620	0.980
1.3	0.04585	0.03070	1.424
1.6	Breakdown	0.04560	1.975

(A) Airspeed = 58 m/s, T_s = −19.8°C, MVD = 20 μm, accretion time = 8 min.
(B) Airspeed = 58 m/s, T_s = −9.67°C, MVD = 20 μm, accretion time = 8 min.

Table 3 Effect of droplet size on drag coefficient

Droplet size, μm	Calculated drag coefficient	Experimental drag coefficient	Equivalent sand-grain roughness, mm
	(A)		
14	0.01283	0.01210	0.334
20	0.01279	0.01930	0.334
26	0.01285	0.01960	0.268
	(B)		
14	0.01578	0.03090	0.934
20	0.04549	0.09510	0.934
26	0.05356	0.12660	0.747

(A) Airspeed = 58 m/s, T_s = −27.8°C, LWC = 1.3 g/m^3, accretion time = 8 min.
(B) Airspeed = 94 m/s, T_s = −12.2°C, LWC = 1.05 g/m^3, accretion time = 6.2 min.

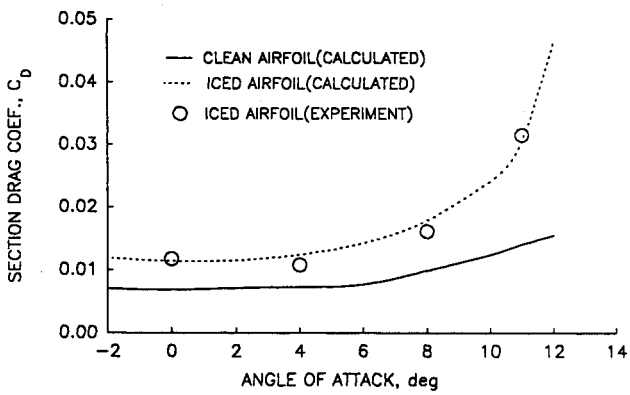

Fig. 10 Variation of the drag coefficient of the airfoil with angle of attack with ice shape determined at α = 4 deg for V_∞ = 58 m/s, T_s = −27.8°C, LWC = 1.0 g/m^3, MVD = 12 μm, ice accretion time = 5 min.

of rime ice, both computed and experimental drag coefficients do not vary much with temperature, but the computed values (around 0.020) are lower than the experimental values (around 0.02). At higher temperatures, the calculated drag coefficient shows a dramatic increase followed by a sudden decrease. In general, the drag coefficients of those iced airfoils, which are of the glaze type, are in good agreement with experiment, despite the breakdown of the IBL calculations at T_s = −6.6°C in Table 1(B). In this case, the calculations capture the increase in the drag coefficient, but not the peak value which may correspond to stall or poststall conditions.

Tables 2(A) and 2(B) show the effect of LWC on drag coefficient. Except at the high values of LWC, the calculations are performed without numerical difficulties and lead to satisfactory results with experimental data. The results are consistent with underprediction of ice buildup in Fig. 4 and overprediction in Fig. 5. Perhaps, as indicated earlier, the calculated drag coefficients can be improved if the predicted ice shapes are brought into a better agreement with measured ones by improving the roughness correlations for LWC.

Tables 3(A) and 3(B) show the effect of droplet size (MVD) on drag coefficient, again for two airspeeds. The results in Table 3(A) contain relatively lower drag coefficients, indicating smaller viscous effects. For the three values of the droplet size, the computed values are in reasonable agreement with the experiment. The experimental drag coefficients of Table 3(B), on the other hand, are very large for the values of MVD ≥ 20, suggesting the existence of increased flow separation and stall and/or poststall conditions. For these

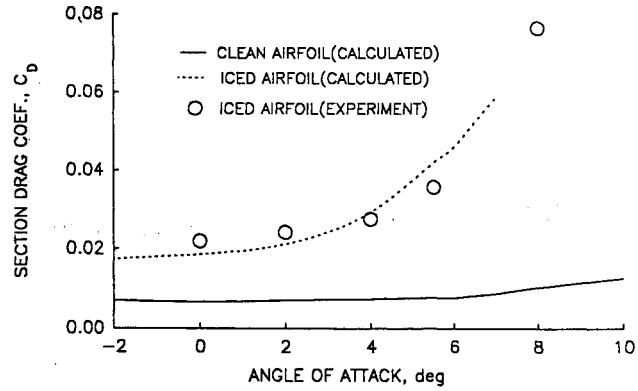

Fig. 11 Variation of the drag coefficient of the airfoil with angle of attack with ice shape corresponding to glaze ice determined at α = 4 deg for V_∞ = 58 m/s, T_s = −9.67°C, LWC = 1.3 g/m^3, MVD = 20 μm, ice accretion time = 5 min.

conditions, the computed values are in poor agreement with data.

Figures 10 and 11 show the variation of the drag coefficient of the airfoil with angle of attack for a given ice shape determined at α = 4 deg. The results in Fig. 10 are for rime ice and indicate remarkably good agreement between calculations and experiment. The increase in the drag coefficient due to the ice is well represented, and the turbulence model with equivalent sand-grain roughness parameters given by Eq. 10 allows the calculations to follow the experimental trend.

The results in Fig. 11 correspond to glaze ice and are again in remarkably good agreement with experimental data, except at higher angles of attack where the code broke down due to the occurrence of stall. It should be noted that the calculations were performed for the ice shape with LWC = 1.3 g/m^3 rather than 2.1 g/m^3 since, according to Fig. 6, the ice shapes in experimental data are not sensitive to LWC. In Figs. 4 and 5, it has already been shown that predicted ice shapes are not in good agreement with data at the higher values of LWC and indicates the need for improved roughness correlations. Since the accuracy of the drag coefficient is a strong function of the ice shape, it is necessary to use a shape that fits the experimental data as well as possible.

Concluding Remarks

The extensive results of the previous section show that the interactive boundary-layer method together with the modified LEWICE code provide a satisfactory basis for the calculation of ice shapes and their effect on airfoil drag. The results encompass a wide range of icing conditions and angles of attack of direct relevance to engineering practice so that the method provides a basis for extension to the representation of icing on wings, other lifting bodies, and engine intakes.

Improvements can be made to the present approach, e.g., to the correlation for equivalent sand-grain roughness and to the representation of the drag coefficient when the ice accretion gives rise to stall or poststall conditions. In the former case, additional measurements and calculations are required, and in the latter a combination of local flow measurements and calculations to examine the sensitivity of the aerodynamic flow characteristics to the time-change in ice shapes. The improvements should be pursued, but should not preclude the immediate extension of the calculation method to deal with three-dimensional lifting bodies and the development of a better heat transfer formulation so that the ice accretion model can also include the effects of surface heating on ice formation.

References

[1]Shaw, R. J., "NASA's Aircraft Icing Analysis Program," NASA TM-88791, Sept. 1987.

[2]Shaw, R. J., Potapczuk, M. G., and Bidwell, C. S., "Predictions of Airfoil Aerodynamic Performance Degradation Due to Ice," *Numerical and Physical Aspects of Aerodynamic Flows, IV.*, edited by T. Cebeci, Springer-Verlag, Long Beach, CA, 1990.

[3]MacArthur, C. D., Keller, J. L., and Leurs, J. K., "Mathematical Modeling of Ice Accretion on Airfoils," AIAA Paper 82-0284, Jan. 1982.

[4]Ruff, G. A., and Berkowitz, B. M., "User's Manual for the NASA Lewis Ice Accretion Prediction Code (LEWICE)," NASA CR-185129, May 1990.

[5]Messinger, B. L., "Equilibrium Temperature of Unheated Icing Surface as a Function of Airspeed," *Journal of Aeronautical Science*, Vol. 20, No. 1, 1953, pp. 29–42.

[6]Cebeci, T., Chen, H. H., and Alemdaroglu, N., "Fortified LEWICE with Viscous Effects," *Journal of Aircraft*, Vol. 28, No. 9, 1991, pp. 564–571.

[7]Potapczuk, M. G., "Navier-Stokes Analysis of Airfoils with Leading-Edge Ice Accretions," Ph.D. Dissertation, Univ. of Akron, Akron, OH, May 1989.

[8]Cebeci, T., "Calculation of Flow over Iced Airfoil," *AIAA Journal*, Vol. 27, No. 7, 1989, pp. 853–861.

[9]Olsen, W., Shaw, R. J., and Newton, J., "Ice Shapes and the Resulting Drag Increase for a NACA 0012 Airfoil," NASA TM-83556, Jan. 1984.

[10]Bradshaw, P., Cebeci, T., and Whitelaw, J. H., *Engineering Calculation Methods for Turbulent Flows*, Academic Press, London, 1981.